Effect on Slender Vehicle Dynamics of Change from Spherical to Conical Nose Bluntness

LARS E. ERICSSON* AND ROLF A. GUENTHER†
Lockheed Missiles & Space Company, Sunnyvale, Calif.

It is by now well established that spherical nose bluntness has a large effect on vehicle dynamics. However, comparatively little data are available for the effect of nonspherical nose bluntness of the shapes resulting from ablative nose tip recession. As the conical nose tip geometry approximates the nose shape expected after ablation under turbulent heating conditions, a previously developed analytical theory for the hypersonic unsteady aerodynamics of spherically blunted cones has been extended to account for the effects of conical nose bluntness. It is found that (ablative) changes from spherical to conical nose bluntness can have significant effects on stability and trim characteristics of slender cones. The theoretical predictions are shown to agree well with available experimental data. It is shown by the theory and verified by experiments that the effects of conical nose bluntness can be represented by universal scaling laws involving two scaling parameters. These scaling laws demonstrate that there exists a critical nose bluntness for which the ablation change from spherical to conical nose-tip has no effect on the vehicle stability derivatives.

Nomenclature

a = speed of sound
c = reference length (cone base diameter, d_B)
d_B = base diameter
d_N = nose (bluntness) diameter
D_N = nose drag coefficient $C_{DN} = D_N/(\rho_\infty U_\infty^2/2)(\pi d_N^2/4)$
f = pressure correlation function
g = velocity ratio, $g = U/U_\infty$
l = sharp cone body length, m (see inset in Fig. 7)
M = Mach number, $M = U/a$
M_p = pitching moment coefficient $C_m = M_p/(\rho_\infty U_\infty^2/2)Sc$
p = static pressure coefficient $C_p = (p - p_\infty)/(\rho_\infty U_\infty^2/2)$
q = rigid body pitch rate
r = body radius (see Fig. 1)
R = radial distance from bow shock centerline (see Fig. 1)
R_{sh} = bow shock radius (see Fig. 1)
S = reference area, $S = \pi c^2/4$
t = time
U = axial velocity
$V_\perp$ = velocity normal to body surface
x = axial body coordinate (see Fig. 1)
x_N = bow shock location (for $M \to \infty$)
$\Delta\bar{x}$ = cone center of gravity location forward of base
Z = inertial space coordinate
z = translatory coordinate (see Fig. 1)
α = angle-of-attack
γ = specific heat ratio ($\gamma = 1.4$ for air)
Δ = difference or increment
θ_c = cone half angle
θ_N = half angle of conical tip
κ_N = hypersonic scaling parameter for nose directing effects defined in Eq. (16)
ρ = air density
ϕ = azimuth location (see Fig. 1)
χ^* = hypersonic similarity parameter defined in Eq. (1c)
χ_l = hypersonic scaling parameter for nose drag effects defined in Eq. (15).

Subscripts

B = base
c = cone
c.g. = center of gravity or oscillation center
max = maximum
N = nose
P = plateau
sh = bow shock
∞ = freestream conditions
o = first body station after the nose
0 = at $\phi = 0$
1 = nondirecting nose bluntness effect, $C_{DN\alpha} = 0$
2 = increment due to nose directing effect, $C_{DN\alpha} \neq 0$

Superscripts

i = induced, e.g., $\Delta^i C_p$ = nose bluntness induced pressure (change) on aft body

Derivative Symbols

$\dot{\alpha} = \partial\alpha/\partial t$
$C_{m\alpha} = \partial C_m/\partial\alpha$
$C_{mq} = \partial C_m/\partial(cq/U_\infty)$; $C_{m\dot{\alpha}} = \partial C_m/\partial(c\dot{\alpha}/U_\infty)$

Introduction

THAT nose bluntness has a large effect on slender cone vehicle dynamics has been well documented by experiments[1-3] and is also predicted theoretically.[4,5] The emphasis of experimental and theoretical research has, however, been on spherical nose bluntness, and comparatively few data are available about the effects of nonspherical nose bluntness. As the ablating re-entry vehicle always will have a nonspherical nose-bluntness during the major portion of its atmospheric trajectory, it is important to know what the effects of nonspherical nose bluntness are.

In the present paper a previously developed analytic theory for spherically blunted slender cones[5] is extended to account for the effects of conical nose bluntness. The conical nose tip geometry approximates the expected vehicle nose shape after ablation under turbulent heating conditions. The spherical nose bluntness characteristics are used as a reference for the effects of conical nose bluntness. The validity of the developed analytic theory for spherical nose bluntness effects[5] has been confirmed by theoretical and experimental research.[3]

Presented as Paper 71–931 at the AIAA Guidance, Control and Flight Mechanics Conference, Hempstead, New York, August 16–18, 1971; submitted September 1, 1971; revision received January 28, 1972.

Index categories: Entry Vehicle Dynamics and Control; Nonsteady Aerodynamics; Supersonic and Hypersonic Flow.

* Senior Staff Engineer. Associate Fellow AIAA.
† Senior Aerodynamics Engineer.

Analytic Approach

The hypersonic inviscid shear flow over the aft body behind a blunt nose is determined by the shape of the bow-shock.[6,7] The shock shape is determined by the nose bluntness and can be related to the nose drag.[8] The Embedded Newtonian shear flow profiles can be represented by one-parameter similar profiles, leading to a simple analytic formulation for the unsteady aerodynamics of blunt cylinder-flare bodies[9] and blunted slender cones.[5]

At angle-of-attack the nose-bluntness-generated "entropy wake" is translated across the "embedded" aft body (Fig. 1). For spherical nose bluntness the nose drag remains constant and the translation of the "entropy wake" is the total nose bluntness induced effect. For conical nose bluntness with the same nose drag (45° nose cone angle), however, the (top and bottom side) nose drag does not remain constant. The decreased top or leeward side nose drag causes a decrease of the entopy wake thus offsetting some of the wake translation effect (Fig. 1). A similar decrease of the wake translation is realized on the windward side. Thus the nose-bluntness induced aft-body loads are decreased when going from spherical to conical nose bluntness (without changing the nose drag).

Another effect of conical nose bluntness is to cut off some of the high blast wave pressures[10] (Fig. 2). The "plateau pressure" is predicted by a pseudo-Prandt-Meyer expansion from fore cone to aft body cone angle (Fig. 3). At angle-of-attack the tangent-cone concept, which is used throughout the present analysis, describes the variation of the plateau pressure and its extent, generating a deviation of the near nose loads from those for spherical nose bluntness. This effect is, however, small unless the nose bluntness is very large. The dominant effect of conical nose bluntness is the nose drag variation discussed earlier, which causes reduced aft body loads.

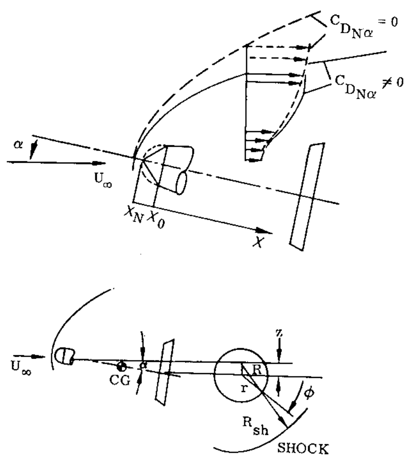

Fig. 1 Nose bluntness-induced entropy wake at small α.

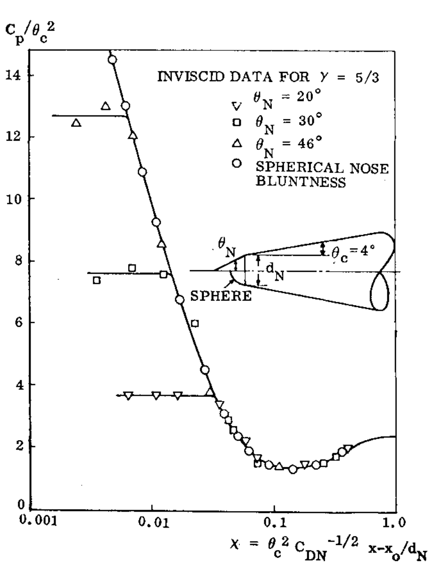

Fig. 2 Pressure distribution over blunted cones at $\alpha = 0$ (Ref. 10).

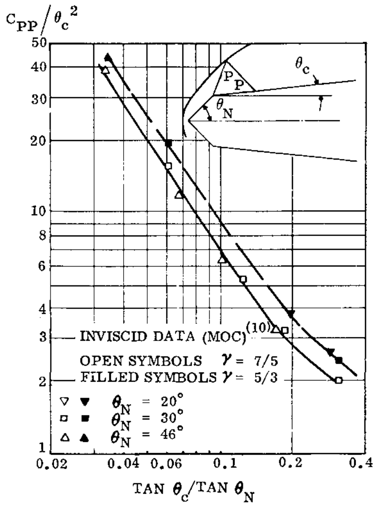

Fig. 3 Plateau pressure in the cone-cone shoulder region at $\alpha = 0$.

Analysis

It has been shown earlier[5–9] that by using hypersonic similarity concepts for the entropy wake, the embedded Newtonian flowfield, the pressure on the conical frustum of a blunted cone can be defined as follows, applying the tangent-cone concept for small α and θ_c:

$$C_p = \frac{0.081\, C_{DN}^{1/2}}{(x/d_N) - (x_N/d_N)} + (V_\perp/U)^2 f(\chi^*) \tag{1a}$$

$$f(\chi^*) = \begin{cases} 0.38 + 2.75\chi^* & : \chi^* \leq 0.5 \\ 2 - 6.86(0.7 - \chi^*)^2 & : 0.5 < \chi^* < 0.7 \\ 2 & : 0.7 \leq \chi^* \end{cases} \tag{1b}$$

$$\chi^* = [(R/d_N) - (1/2)]^2/C_{DN}^{1/2}[(x/d_N) - (x_N/d_N)] \tag{1c}$$

$$\left(\frac{R}{d_N}\right)^2 = \left(\frac{z}{d_N}\right)^2 + 2\left(\frac{z}{d_N}\right)\cos\alpha\left[\frac{1}{2} + \frac{x - x_o}{d_N}\,\theta_c\right]\sin\phi + \left(\frac{1}{2} + \frac{x - x_o}{d_N}\,\theta_c\right)^2 [\cos^2\alpha \sin^2\phi + \cos^2\phi] \tag{1d}$$

$$\frac{V_\perp}{U} = \theta_c + \alpha\sin\phi + \left[\frac{x}{d_N} - \frac{x_{CG}}{d_N} + \left(\frac{1}{2} + \frac{x - x_o}{d_N}\,\theta_c\right)\theta_c\right]\frac{d_N q}{U}\sin\phi \tag{1e}$$

Differentiating Eq. (1) with respect to α gives the following derivatives‡

$$C_{p\alpha} = (C_{p\alpha L})_1 + (C_{p\alpha L})_2 + (\Delta^i C_{p\alpha})_1 + (\Delta^i C_{p\alpha})_2 \tag{2a}$$

$$(C_{p\alpha L})_1 = 2\theta_c f(\chi^*)[1 + (\alpha/\theta_c)\sin\phi]\sin\phi \tag{2b}$$

$$(C_{p\alpha L})_2 = \{0.081/2C_{DN}^{1/2}[(x/d_N) - (x_N/d_N)]\}(dC_{DN}/d_\alpha) \tag{2c}$$

$$(\Delta^i C_{p\alpha})_1 = 2\theta_c^2\chi^*\frac{\partial f}{\partial \chi^*}\left[1 + \left(\frac{\alpha}{\theta_c}\right)\sin\phi\right]^2 \times \frac{z/d_N + \{1/2 + [(x - x_0)/d_N]\theta_c\}\sin\phi}{(R/d_N)(R/d_N - 1/2)}\,\frac{d(z/d_N)}{d\alpha} \tag{2d}$$

$$(\Delta^i C_{p\alpha})_2 = -0.5\theta_c^2\chi^*\frac{\partial f}{\partial \chi^*}\,\frac{d(\log C_{DN})}{d\alpha}\left[1 + \left(\frac{\alpha}{\theta_c}\right)\sin\phi\right]^2 \tag{2e}$$

‡ The authors are thankful to O. Walchner for pointing out a mistake in the expression for $(\Delta^i C_{p\alpha})_2$ in Preprint AIAA 71-931.

It is $dC_{DN}/d\alpha$ in Eq. (2) which expresses the attitude sensitivity of the conical nose bluntness. In the local component $(C_{p\alpha L})_2$ the effect of $dC_{DN}/d\alpha$ is to change the radial distance to the bow shock, thereby changing the dynamic pressure profile as expressed through $f(\chi^*)$.

Using the tangent cone concept and the modified Newtonian theory, the nose drag (for the ϕ-slice) is defined as follows.

$$C_{DN} = \frac{8}{d_N^2}\int_{x_N}^{x_0} C_p \tan(\theta + \alpha\sin\phi) r dx;\; C_p = C_{p\max}\sin^2(\theta + \alpha\sin\phi) \quad (3)$$

For a conical nose tip, $\theta = \theta_N =$ constant, the nose drag characteristics are (for small angles of attack)

$$C_{DN} = C_{p\max}\sin^2(\theta_N + \alpha\sin\phi);\; (dC_{DN}/d\alpha) = C_{p\max}\sin 2(\theta_N + \alpha\sin\phi)\sin\phi \quad (4)$$

At $\alpha = 0$ the nose drag derivative becomes simply

$$(dC_{DN}/d\alpha) = (dC_{DN}/d\alpha)_0\sin\phi;\; (dC_{DN}/d\alpha)_0 = C_{p\max}\sin 2\theta_N \quad (5)$$

Differentiating Eq. (1) with respect to (cq/U_∞) gives the dynamic derivative due to local pitch rate.

$$\left.\begin{aligned} C_{pq} &= \frac{\partial C_p}{\partial\left(\dfrac{cq}{U_\infty}\right)} = 2\frac{f(\chi^*)}{g(\chi^*)}\left(\frac{d_N}{c}\right)\theta_c\left[1 + \left(\frac{\alpha}{\theta_c}\right)\sin\phi\right]\times \\ &\quad \left[\left(\frac{x}{d_N} - \frac{x_{CG}}{d_N}\right) + \left(\frac{1}{2} + \frac{x - x_o}{d_N}\theta_c\right)\theta_c\right]\sin\phi \\ g(\chi^*) &= \frac{U}{U_\infty} = \begin{cases} 0.68 + 0.42\chi^{*1/2}: & \chi^* < 0.5 \\ 1 & : 0.5 \le \chi^* \end{cases} \end{aligned}\right\} \quad (6)$$

The dynamic $\dot\alpha$-derivative, which is generated by convective time-lag effects, can be obtained from the variation with time of the induced pressure $\Delta^i C_p$

$$\Delta^i C_p(t) = \frac{\partial\Delta^i C_p}{\partial\left(\dfrac{z}{d_N}\right)}\left[\frac{Z(x,t)}{d_N} - \frac{Z(x_0, t - \Delta t)}{d_N}\right] + \frac{\partial\Delta^i C_p}{\partial C_{DN}}\frac{dC_{DN}}{d\alpha}\alpha(t - \Delta t) \quad (7)$$

The time Δt is the time lag occurring before the effects of perturbations at the nose (x_o) have been convected downstream to the submerged body element (x).

$$\Delta t = (x - x_o)/U = (x - x_o)/U_\infty g(\chi^*) \quad (8)$$

For a rigid body, z is (for small α)

$$z = Z(x) - Z(x_o);\; Z = Z_{CG} + (x - x_{CG})\alpha \quad (9)$$

and Eq. (7) can be written:

$$\Delta^i C_p(t) = \frac{\partial\Delta^i C_p}{\partial\left(\dfrac{z}{d_N}\right)}\left[\frac{x - x_{CG}}{d_N}\alpha(t) - \frac{x_o - x_{CG}}{d_N}\alpha(t - \Delta t)\right] + \frac{\partial\Delta^i C_p}{\partial C_{DN}}\frac{dC_{DN}}{d\alpha}\alpha(t - \Delta t) \quad (10)$$

For slow oscillations, $(c\dot\alpha/U_\infty)^2 \ll 1$, $\alpha(t - \Delta t)$ is given by the first terms in a Taylor expansion, i.e.,

$$\alpha(t - \Delta t) = \alpha(t) - \dot\alpha(t)\Delta t \quad (11)$$

Thus, Eq. 10 can be written in the following form:

$$\Delta^i C_p(t) = \frac{\partial\Delta^i C_p}{\partial\left(\dfrac{z}{d_N}\right)}\frac{d\left(\dfrac{z}{d_N}\right)}{d\alpha}\left\{\alpha + \left[\frac{x_o - x_{CG}}{c}\Big/ g(\chi^*)\right]\frac{c\dot\alpha}{U_\infty}\right\} + \frac{\partial\Delta^i C_p}{C_{DN}}\frac{dC_{DN}}{d\alpha}\left\{\alpha - \left[\frac{x - x_o}{c}\Big/ g(\chi^*)\right]\frac{c\dot\alpha}{U_\infty}\right\} \quad (12)$$

The dynamic $\dot\alpha$ derivative is given as

$$\Delta^i C_{p\dot\alpha} = \frac{\partial\Delta^i C_p(t)}{\partial(c\dot\alpha/U)} = (\Delta^i C_{p\alpha})_1\left(\frac{x_o}{c} - \frac{x_{CG}}{c}\right)\Big/ g(\chi^*) + (\Delta^i C_{p\alpha})_2\left(\frac{x_o}{c} - \frac{x}{c}\right)\Big/ g(\chi^*) \quad (13)$$

The normal force and moment derivative contributions from the conical frustum can be determined from the above expressions for the C_p-derivatives. The contribution from the nose itself is computed using modified Newtonian Theory.

Discussion of Results

As was indicated earlier, the main effect of a change from spherical to conical nose bluntness, while keeping the nose drag constant ($\theta_N = 45°$), is to change the aft body loads induced by the nose bluntness (Fig. 4). Only for very large nose bluntness ratios will the modification of local loads at the cone-cone shoulder become important. Difference in local nose tip loads will be much more important, judging from the Newtonian (sharp cone) load level at the shoulder. The load modification due to the conical nose tip, the negative load distribution, will increase stability if the center of gravity is downstream of its centroid location, $(x - x_o)/d_N \approx 10$ in Fig. 4, and will decrease the static stability when the c.g. is upstream of this location. This critical $(x_{c.g.}/d_N)$-value corresponds to a critical bluntness ratio

$$(x_{c.g.}/d_N)_{crit}l = (x_{c.g.}/l)/2\tan\theta_c(d_N/d_B)_{crit} \quad (14)$$

This is confirmed by the data in Fig. 5. The present predictions agree rather well with recent experimental results,[12] especially when considering the small static margin and associated large scatter of the data in Fig. 5. Because of the convective time lag effects, associated with the nose bluntness induced effects, reversed reactions are exhibited by dynamic and static characteristics.[5] Where the conical nose tip increases static stability, $(d_N/d_B) \le 0.15$, it decreases the dynamic stability, and vice versa for $(d_N/d_B) > 0.15$. If there had been experimental dynamic data available, we would have expected them to confirm this predicted reversed effect. When the conical tip effect is concentrated to the forebody, $d_N/d_B \le 0.15$, the dynamic amplification factor $(x_o - x)$ in Eq. (13) is small, and the change from spherical to conical nose tip will increase static stability without incurring any appreciable loss of dynamic stability. At $d_N/d_B > 0.15$ the dynamic amplification becomes large. However, much of the effect shown in Fig. 5 is due to the sharply decreased magnitude of the normalizing value, the damping derivative of a spherically blunted cone (see Fig. 7).

The use of spherical nose bluntness data as a norm for the evaluation of conical nose bluntness effect is based upon the following more or less well established facts. It is very

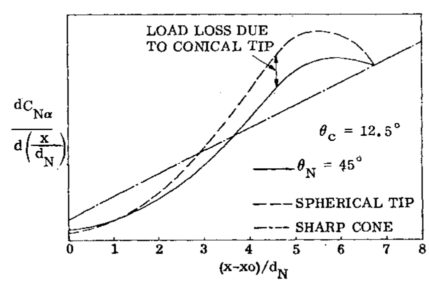

Fig. 4 Effect of conical bluntness geometry on frustum loads at $\alpha = 0$.

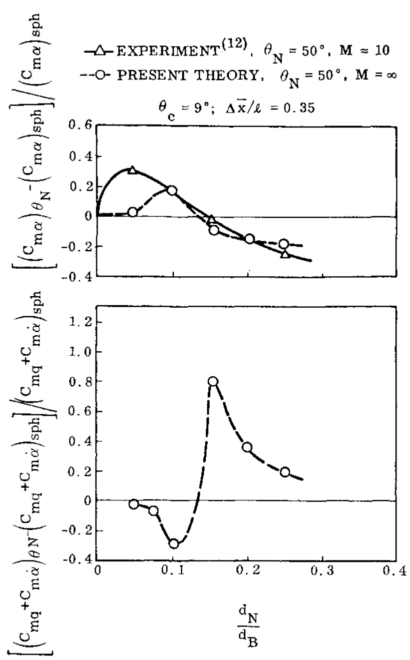

Fig. 5 Effect of 50° conical nose bluntness on stability derivatives of 9° cone.

difficult to compare inviscid predictions with viscous experimental data, especially when the tests are run at hypersonic low density conditions. Boundary-layer cross flow becomes very important[13] and support interference may distort the data, especially in dynamic tests.[14] It was shown in Ref. 5 that if experimental and theoretical data were normalized by use of sharp cone data, thus eliminating boundary layer cross-flow effects that are common to both sharp and spherically blunted cones,§ good agreement was found to exist between the analytic predictions by the present method and available experimental data. Since then the present analytic method has been checked further in regard to its capability to predict the aerodynamic characteristics for spherically blunted cones. The present analytic method agrees well with the much more time consuming method of characteristics,[15] and both methods predict the experimental data obtained in wind tunnel and ballistic range tests.[3]

Thus, the veracity of the present theory in predicting the effects of spherical nose bluntness is well documented. In regard to the effects of nonspherical nose bluntness, the analysis presented here, Eqs. (1–14), shows that the basic nose drag effect of frustum loads (constant C_{DN}) is insensitive to shape. Consequently, that portion of the nose bluntness induced effect should by predicated as well for conical as for spherical nose bluntness. The new effect induced by a conical nose tip is the attitude sensitivity of the nose drag, $C_{DN\alpha} \neq 0$. As a spherical and a 45° conical nose tip have the same drag, the difference shown in Fig. 4 is caused entirely by the nose-tip-directing $C_{DN\alpha}$-effect. This is also to a large extent true for the data shown in Fig. 5, where $\theta_N = 50°$ rather than $\theta_N = 45°$. That is, the experimental data in Fig. 5 confirm the effects of nonspherical nose bluntness predicted by the present theory.

This confirmation would not have been obtained in a direct comparison between inviscid theory and (viscous) experiments. In addition to preventing boundary layer cross flow effects and support interference from distorting the comparison, using incremental characteristics also eliminates those strong viscous interaction effects near the nose[16] that are common to both spherical and conical nose tips.

§ In the near nose region the cross flow effects are not similar to those for a sharp cone and this similarity is therefore good only for moderately blunt slender cones.

The effect of nose cone angle θ_N on the bluntness induced frustum loads on a 9° cone is shown in Fig. 6. As can be seen, the effects are substantial. The data show the total effect of nose cone angle, i.e., both the change of C_{DN} and the $C_{DN\alpha}$-effect are included. When trying to compare different sets of experimental data one runs into one very common problem: usually more than one of the significant parameters, i.e., cone angle (θ_c), nose shape (spherical or conical θ_N), bluntness ratio (d_N/d_B), and center of gravity, ($x_{c.g.}/l$), is changed between different tests. This makes it difficult to evaluate what the effect of one single parameter is, e.g., the nose shape. One needs a scaling parameter that includes the effects of more than one of the basic parameters mentioned above. Because of the simplicity of the embedded Newtonian concept used in the present analysis, it was found possible to formulate such a scaling parameter for the effects of spherical nose bluntness.[11]

$$\chi_l = (\tan\theta_c/2)/(d_N/d_B)C_{DN}^{1/2} \tag{15}$$

For spherical nose bluntness (and for $\theta_N = 45°$) modified Newtonian theory gives $C_{DN} = 0.90$. Thus, for slender (θ_c small) spherically blunted cones the scaling parameter $\chi_l^{-1} = 1.9\ (d_N/d_B)/\theta_c$ accounts for the combined effect of bluntness ratio and frustum cone angle, and data for the same center of gravity are represented by one universal curve. Cone angles of 5, 5.6, 6, 6.3, 7.25, 9, 10, and 12.5 degs have been used in combinations with nose bluntnesses from zero up to $d_N/d_B = 0.40$. All these individual pieces of valuable data can now be combined to define this universal curve for experimentally determined effects of nose bluntness on slender cone vehicle dynamics. Figure 7 shows only the experimental data available in the open literature.[1,2] One might, of course, expect the curve to change somewhat as more data becomes available. However, this universal curve for the experimental data agrees rather well with predictions made by the analytic theory that helped formulate this scaling parameter.[5,11] The deviation is consistent with the viscous-induced effective increase of nose

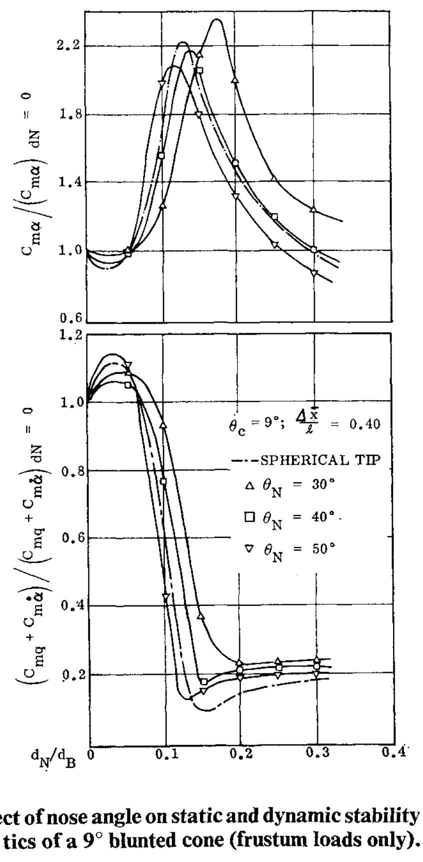

Fig. 6 Effect of nose angle on static and dynamic stability characteristics of a 9° blunted cone (frustum loads only).

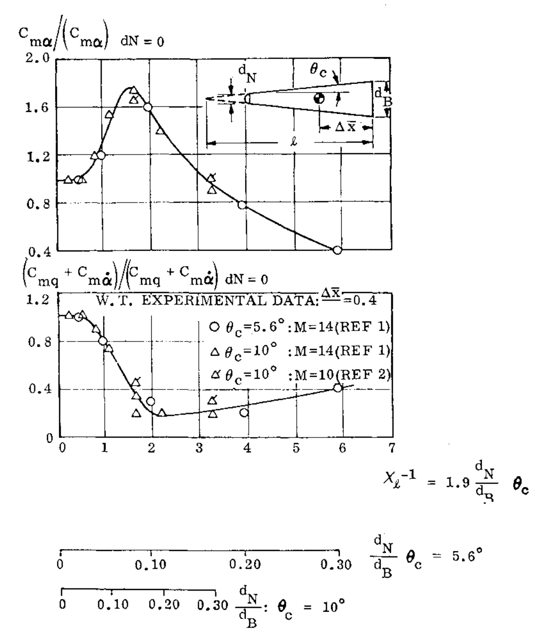

Fig. 7 Universal scaling of spherical nose bluntness effects.

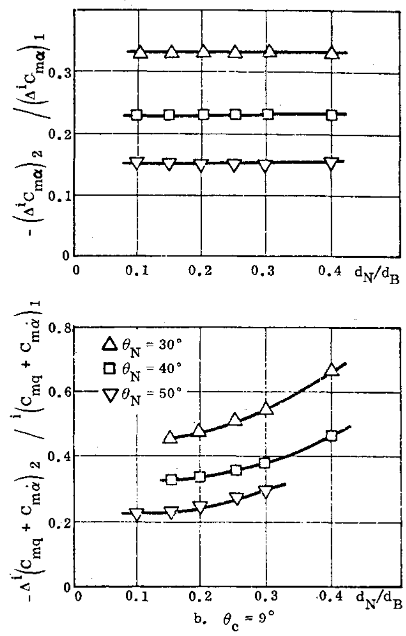

Fig. 9 Nose-tip-directing ($C_{DN\alpha}$) effects on stability of a 9° blunted cone.

bluntness[11,16] that still remains after "normalizing" of the experimental data.

The data in Fig. 6, removed of the $C_{DN\alpha}$-effect (i.e., showing only the effect of a constant C_{DN} corresponding to the nose cone angle θ_N), are shown in Fig. 8 plotted against the scaling parameter χ_l^{-1}. In accordance with the expectations expressed earlier in discussing Figs. 4 and 5, the data are well represented by one universal curve. The amplification of the nose drag induced frustum loading by the $C_{DN\alpha}$-effect is shown in Fig. 9 against the same scaling parameter. The data seem to be ordered along the horizontal coordinate χ_l^{-1}. However, the $C_{DN\alpha}$-effect is dependent not only upon θ_c but also upon θ_N. In order to organize the data along the vertical axis, we need an additional scaling parameter for this combined effect of θ_N and θ_c.

Examining Eqs. (2 and 5) one finds that for $\alpha = 0$ the ratio between the $C_{DN\alpha}$-effect on frustum pressure, $(\Delta^i C_{p\alpha})_2$, and the constant nose drag effect, $(\Delta^i C_{p\alpha})_1$, can be formulated as follows:

$$\kappa_N = [(\Delta^i C_{p\alpha})_2/(\Delta^i C_{p\alpha})_1] = -[(C_{DN\alpha})_0/C_{DN0}][\theta_c/4] \qquad (16)$$

For conical nose bluntness κ_N becomes¶

$$\kappa_N = -(1/2)(\tan\theta_c/\tan\theta_N)$$

Thus, if the data in Fig. 8 are normalized through dividing by κ_N, the $C_{DN\alpha}$-effects are represented by one universal curve (Fig. 10). When κ_N is close to 45°, κ_N scales also the nose directing effect normalized to spherical nose bluntness characteristics (Fig. 11). The combined usage of Figs. 8 and 10

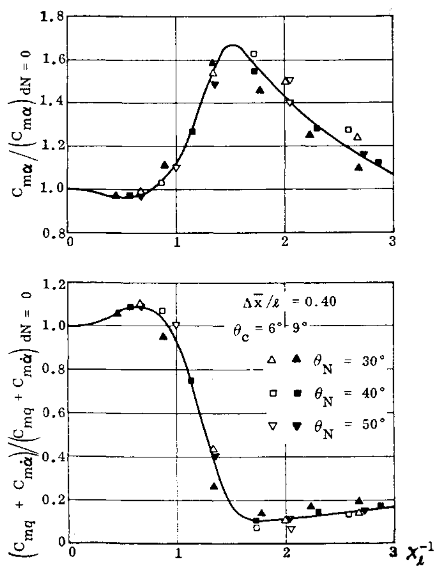

Fig. 8 Conical nose drag effects on stability characteristics of slender nose cones (frustum loads only).

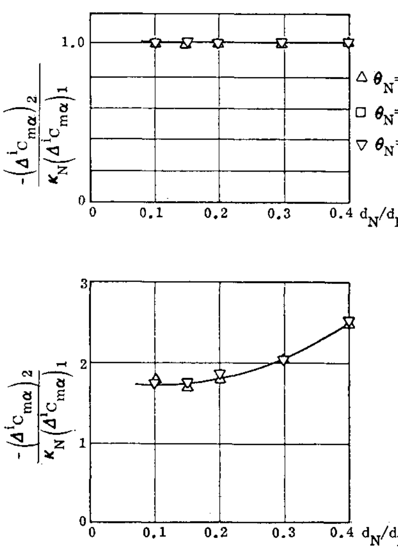

Fig. 10 Universal scaling of nose-tip-directing ($C_{DN\alpha}$) effects for 6° and 9° cones (frustum loads only).

¶ Throughout the analysis in this paper it is assumed that θ_c is small. ($\sin\theta_c = \tan\theta_c = \theta_c$.) Note that $-2\kappa_N$ also correlates the plateau pressure in the cone-cone shoulder region (Fig. 3).

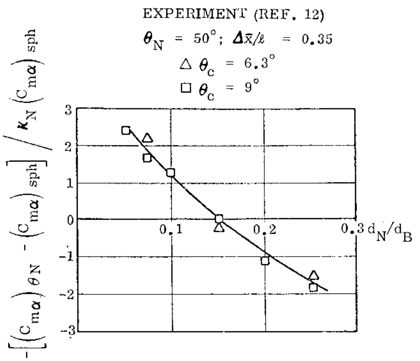

Fig. 11 Universal scaling of nose-tip-directing ($C_{DN\alpha}$) effects for $\theta_N = 50°$.

or 11 will provide the contribution from frustum loads to the stability characteristics for a slender cone with arbitrary θ_c and θ_N. The local nose lift is accounted for simply by use of modified Newtonian theory ($C_{p\max} = 1.8$).

Conclusions

An analysis has shown that ablation induced shape changes, from initially spherical to conical nose tips, can have large effects on the stability characteristics of slender cones. The results can be summarized as follows. 1) The developed analytic theory predicts the experimentally observed static and dynamic stability characteristics of slender cones with conical nose bluntness. 2) Changing from spherical to conical nose bluntness without a change of nose drag ($\theta_N = 45°$) will increase static stability for moderate nose bluntness and decrease it for large nose bluntness. The effects on dynamic stability are opposite, causing some decrease for small and a substantial increase for large nose bluntness. 3) There exists a critical nose bluntness such that ablative changes from spherical to conical nose bluntness have no effect on the vehicle stability. 4) The effect of conical nose bluntness can be represented by uniquely valid relationships using two scaling parameters, thus permitting "analytic extrapolation" from one set of experimental data to blunted cones with different nose cone and frustum angles.

References

[1] Walchner, O. and Clay, J., "Nose Bluntness Effects on the Stability Derivatives of Cones in Hypersonic Flow," *Transactions of the Second Technical Workshop on Dynamic Stability Testing*, Arnold Engineering Development Center, Arnold Air Force Station, Tullahoma, Tenn., Vol. 1, Paper 8, April 20–22, 1965.

[2] Ward, L. K. Jr. and Uselton, B. L., "Dynamic Stability Results for Sharp and Blunted 10-Deg. Cones at Hypersonic Speeds", *Transactions of the 3rd Technical Workshop on Dynamic Stability Problems*, Vol. III, Paper 2, Nov. 4–7, 1968, NASA Ames Research Center, Moffett Field, Calif.

[3] Malcolm, G. N. and Rakich, J. V., "Comparison of Free-Flight Experimental Results and Theory on the Nonlinear Aerodynamic Effects of Bluntness for Slender Cones," *AIAA Journal*, Vol. 9, No. 3, March 1971, pp 473–478.

[4] Rie, H., Linkievicz, E. A., and Bosworth, F. D., "Hypersonic Dynamic Stability, Part III, Unsteady Flow Field Program," FDL-TDR-64-149, Part III., Jan. 1967, Air Force Flight Dynamics Lab., Wright-Patterson Air Force Base, Ohio.

[5] Ericsson, L. E., "Effect of Nose Bluntness, Angle of Attack, and Oscillation Amplitude on Hypersonic Unsteady Aerodynamics of Slender Cones," *AIAA Journal*, Vol. 9, No. 2, Feb. 1971, pp. 297–304.

[6] Seiff, A. and Whiting, E. E., "Calculation of Flow Fields from Bow-Wave Profiles for the Downstream Region of Blunt-Nosed Circular Cylinders in Axial Hypersonic Flight," TND-1147, 1961, NASA.

[7] Seiff, A., "Secondary Flow Fields Embedded in Hypersonic Shock Layers," TND-1304, 1962, NASA.

[8] Seiff, A. and Whiting, E. E., "A Correlation Study of the Bow-Wave Profiles of Blunt Bodies," TND-1148, 1962, NASA.

[9] Ericsson, L. E., "Unsteady Aerodynamics of an Ablating Flared Body of Revolution including Effects of Entropy Gradient," *AIAA Journal*, Vol. 6, No. 12, Dec. 1968, pp. 2395–2401.

[10] Wagner, R. D. Jr. and Watson, R., "Induced Pressures and Shock Shapes on Blunt Cones in Hypersonic Flow", TND-2182, 1964, NASA.

[11] Ericsson, L. E., "Universal Scaling Laws for Hypersonic Nose Bluntness Effects," *AIAA Journal*, Vol. 7, No. 12, Oct. 1969, pp. 2222–2227.

[12] Neff, R. S., "Conical Nose Shape Effects on Drag and Static Stability at Mach 10," *Journal of Spacecraft and Rockets*, Vol. 9, No. 2, Feb. 1972, pp. 126–128.

[13] Rakich, J. V. and Cleary, J. W., "Theoretical and Experimental Study of Supersonic Flow Around Inclined Bodies of Revolution," *AIAA Journal*, Vol. 8, No. 3, March 1970, pp. 511–518.

[14] Reding, J. P. and Ericsson, L. E., "Dynamic Support Interference—Fact or Fiction?" AIAA Paper 71-277, AIAA Aerodynamic Testing Conference, Albuquerque, New Mexico, March 10–12, 1971.

[15] Rakich, J. V., "Numerical Calculation of Supersonic Flows of a Perfect Gas over Bodies of Revolution at Small Angles of Yaw," TND-2390, 1964, NASA.

[16] Friberg, E. G. and Walchner, O., "Pressure Correlation for Blunted Slender Cones," *AIAA Journal*, Vol. 7, No. 8, Aug. 1969, pp. 1618–1619.